Dyes and Pigments 91 (2011) 446–453

Contents lists available at ScienceDirect

Dyes and Pigments

journal homepage: www.elsevier.com/locate/dyepig

Synthesis, X-ray crystal structure and optical properties of novel 2,5-diaryl-1,3,4-oxadiazole derivatives containing substituted pyrazolo[1,5-*a*]pyridine units

He Yang [a], Jinglin Mu [a], Xia Chen [a], Lei Feng [a], Jiong Jia [b,*], Jianwu Wang [a,*]

[a] School of Chemistry and Chemical Engineering, Shandong University, 27 Shanda Nanlu, Jinan 250100, Shandong, PR China
[b] State Key Laboratory of Crystal Materials, Shandong University, Jinan 250100, PR China

ARTICLE INFO

Article history:
Received 21 December 2010
Received in revised form
27 March 2011
Accepted 30 March 2011
Available online 13 April 2011

Keywords:
Pyrazolo[1,5-*a*]pyridine
1,3,4-Oxadiazole
Fluorescence
Absorption
Crystal structure
Heterocycle

ABSTRACT

A series of pyrazolo[1,5-*a*]pyridine-containing 2,5-diaryl-1,3,4-oxadiazole derivatives were synthesized and their structures were characterized by IR, ^{1}H NMR and HRMS spectra. The crystal structure of **3a** was determined using single crystal X-ray crystallography. Its spatial structure was found to be monoclinic, and all aromatic rings were approximately coplanar, which allowed conjugation. The absorption results showed that compounds **1a**–**f** presented their absorption peaks ranging from 264 nm to 290 nm, while compounds **3a**–**f** with a larger conjugation system exhibited red-shifted absorption character (absorption maxima between 283 nm and 303 nm) compared to the corresponding absorption of **1a**–**f**. Fluorescence spectra revealed that these compounds exhibited blue fluorescence (421–444 nm) in dilute solutions and showed quantum yields of fluorescence between 0.32 and 0.83 in dichloromethane.

1. Introduction

2,5-Diaryl-1,3,4-oxadiazoles have enjoyed widespread use in organic electronics. Due to the electron-deficient property of 1,3,4-oxadiazole derivatives, as well as good thermal stabilities and high photoluminescence quantum yields [1], 2,5-diaryl-1,3,4-oxadiazoles are the famous electron-transporting and emitting materials for organic light emitting diodes (OLEDs) [2–6]. In recent years, many two-photon absorption (TPA) molecules containing oxadiazole segment as the electron-accepting group have been synthesized and investigated [7–10]. In addition, oxadiazole-based materials have been also applied in organic field-effect transistors (OFETs) [11,12] and molecular level devices and machines [13,14].

Pyrazolo[1,5-*a*]pyridine derivatives are nitrogen-containing heterocycles and have been of particular interest for their pharmacological and biological activities. Of these heterocycles, 2-substituted pyrazolo[1,5-*a*]pyridine derivatives have been shown to be effective dopamine D3 and D4 receptor antagonists [15–18], adenosine A1 receptor antagonists [19], p38 kinase inhibitors [20] and EphB3 receptor tyrosine kinase inhibitors [21]. They have been also reported to exhibit potent activity against herpesviruses [22,23]. The azaindole-like pyrazolo[1,5-*a*]pyridine ring has a large dipole moment due to the non-uniform charge distribution in the five-membered and six-membered rings (Fig. 1). Within the pyrazolo[1,5-*a*]pyridine ring, electronic charge builds up significantly in the five-membered ring while low electron density appears in the six-membered ring. Conjugated organic compounds with large polarizabilities are of particular use in the field of optical electronics, such as non-linear optics [24]. To date little attention has been paid to the photophysical properties of these pyrazolo[1,5-*a*]pyridine derivatives. Thus, as a continuation of our efforts in synthesizing nitrogen-bridgehead heterocycles and exploring novel fluorescent nitrogen-containing compounds [25,26], we would like to synthesize a series of pyrazolo[1,5-*a*]pyridine-containing 2,5-diaryl-1,3,4-oxadiazole derivatives with both potential bioactivities and optical characters and investigate their structural and spectroscopic properties.

2. Materials and methods

2.1. General

All reagents were commercially available and used without further purification. Melting points were recorded on an XD-4 digital micro melting point apparatus and uncorrected. ^{1}H NMR

* Corresponding authors. Tel.: +86 531 88362708; fax: +86 531 88564464.
E-mail addresses: jiongjia@sdu.edu.cn (J. Jia), jwwang@sdu.edu.cn (J. Wang).

0143-7208/$ – see front matter © 2011 Elsevier Ltd. All rights reserved.
doi:10.1016/j.dyepig.2011.03.035

Fig. 1. Charge distribution within pyrazolo[1,5-*a*]pyridine moiety.

spectra were recorded on a Bruker Avance 300 MHz spectrometer, using $CDCl_3$ or d_6-DMSO as solvent and TMS as internal standard. IR spectra were recorded with an IR spectrophotometer VERTEX 70 FT-IR (Bruker Optics). HRMS spectra were recorded on a Q-TOF6510 spectrograph (Agilent). UV–vis spectra were recorded on a U-4100 (Hitachi) spectrophotometer. Fluorescent measurements were recorded on a Perkin–Elmer LS-55 luminescence spectrophotometer.

2.2. Synthesis

2.2.1. General procedure for the synthesis of **1a–f**

Compounds **1a**, **1b** and **1f** were synthesized using the same method for **1c**, **1d** and **1e** we reported before [25].

*2.2.1.1. Ethyl 2-(3,4-dimethoxyphenyl)-pyrazolo [1,5-a]pyridine-5-carboxylate (**1a**).* Yellow solid, yield 61%, mp 190–191 °C. IR (KBr) ν/cm^{-1}: 3056 (ArH), 1709 (C=O), 1485 (Ar), 1269 (C–O–C), 760 (ArH); ^{1}H NMR (300 MHz, $CDCl_3$): δ 8.45–8.48 (d, J = 7.2 Hz, 1H, ArH), 8.26 (s, 1H, ArH), 7.56 (d, J = 1.8 Hz, 1H, ArH), 7.48–7.51 (m, 1H, ArH), 7.29–7.32 (dd, J_1 = 7.2 Hz, J_2 = 1.8 Hz, 1H, ArH), 6.93–6.97 (m, 2H, ArH), 4.38–4.45 (q, J = 7.2 Hz, 2H, CH_2), 4.01 (s, 3H), 3.94 (s, 3H), 1.40–1.45 (t, J = 7.2 Hz, 3H, CH_3); HRMS calcd for $[M + H]^+$ $C_{18}H_{19}N_2O_4$: 327.1345; found: 327.1346.

*2.2.1.2. Ethyl 2-(4-biphenyl)-pyrazolo [1,5-a]pyridine-5-carboxylate (**1b**).* White solid, yield 68%, mp 201–202 °C. IR (KBr) ν/cm^{-1}: 3052 (ArH), 1713 (C=O), 1474 (Ar), 1269 (C–O), 760 (ArH); ^{1}H NMR (300 MHz, $CDCl_3$): δ 8.48–8.50 (d, J = 7.2 Hz, 1H, ArH), 8.29 (s, 1H, ArH), 8.03–8.05 (m, 2H, ArH), 7.64–7.71 (m, 4H, ArH), 7.43–7.48 (m, 2H, ArH), 7.31–7.39 (m, 2H, ArH), 7.02 (s, 1H, ArH), 4.38–4.45 (q, J = 7.2 Hz, 2H, CH_2), 1.41–1.45 (t, J = 7.2 Hz, 3H, CH_3); HRMS calcd for $[M + H]^+$ $C_{22}H_{19}N_2O_2$: 343.1447; found: 343.1443.

*2.2.1.3. Ethyl 2-(naphthalen-2-yl)-pyrazolo [1,5-a]pyridine-5-carboxylate (**1f**).* White solid, yield 70%, mp 178–179 °C. IR (KBr) ν/cm^{-1}: 3051 (ArH), 1709 (C=O), 1528 (Ar), 1256 (C–O), 750 (ArH); ^{1}H NMR (300 MHz, $CDCl_3$): δ 8.48–8.50 (m, 1H, ArH), 8.43 (s, 1H, ArH), 8.28 (s, 1H, ArH), 8.06–8.09 (m, 1H, ArH), 7.90–7.93 (m, 2H, ArH), 7.83–7.86 (m, 1H, ArH), 7.47–7.58 (m, 2H, ArH), 7.30–7.33 (m, 1H, ArH), 7.08 (s, 1H, ArH), 4.37–4.46 (m, 2H, CH_2), 1.40–1.45 (m, 3H, CH_3); HRMS calcd for $[M + H]^+$ $C_{20}H_{17}N_2O_2$: 317.1290; found: 317.1291.

2.2.2. General procedure for the synthesis of **2a–f**

A mixture of compound **1** (3 mmol) and 80% hydrazine monohydrate (10 mL) was maintained under reflux for 6 h. After the solution was cooled, white solid was precipitated. The crude product was filtered and washed with ethanol to afford compound **2** as white crystals.

*2.2.2.1. 2-(3,4-Dimethoxyphenyl)-pyrazolo [1,5-a]pyridine-5-carbohydrazide (**2a**).* White solid, yield 89%, mp 215–216 °C. ^{1}H NMR (300 MHz, d_6-DMSO): δ 10.00 (s, 1H, NH), 8.73–8.76 (d, J = 7.2 Hz, 1H, ArH), 8.14 (s, 1H, ArH), 7.55–7.57 (d, J = 7.2 Hz, 2H, ArH), 7.21–7.24 (m, 2H, ArH), 7.04–7.07 (m, 1H, ArH), 4.61 (s, 2H, NH_2), 3.86 (s, 3H, OCH_3), 3.81 (s, 3H, OCH_3); HRMS calcd for $[M + H]^+$ $C_{16}H_{17}N_4O_3$: 313.1301; found: 313.1308.

*2.2.2.2. 2-(4-Biphenyl)-pyrazolo [1,5-a]pyridine-5-carbohydrazide (**2b**).* White solid, yield 92%, mp 219–220 °C. ^{1}H NMR (300 MHz, d_6-DMSO): δ 10.01 (s, 1H, NH), 8.77–8.83 (m, 1H, ArH), 8.38 (s, 1H, ArH), 8.09–8.20 (m, 2H, ArH), 7.74–7.83 (m, 4H, ArH), 7.29–7.52 (m, 5H, ArH), 4.61 (s, 2H, NH_2); HRMS calcd for $[M + H]^+$ $C_{20}H_{17}N_4O$: 329.1402; found: 329.1406.

*2.2.2.3. 2-(4-Fluorophenyl)-pyrazolo [1,5-a]pyridine-5-carbohydrazide (**2c**).* White solid, yield 84%, mp 247–248 °C. ^{1}H NMR (300 MHz, d_6-DMSO): δ 10.00 (s, 1H, NH), 8.75–8.78 (d, J = 7.2 Hz, 1H, ArH), 8.18 (s, 1H, ArH), 8.01–8.04 (m, 2H, ArH), 7.50–7.56 (m, 2H, ArH), 7.27–7.30 (m, 2H, ArH), 4.60 (s, 2H, NH_2); HRMS calcd for $[M + H]^+$ $C_{14}H_{12}FN_4O$: 271.0995; found: 271.0992.

*2.2.2.4. 2-(4-Chlorophenyl)-pyrazolo [1,5-a]pyridine-5-carbohydrazide (**2d**).* White solid, yield 80%, mp 233–234 °C. ^{1}H NMR (300 MHz, d_6-DMSO): δ 10.00 (s, 1H, NH), 8.75–8.78 (d, J = 7.2 Hz, 1H, ArH), 8.18 (s, 1H, ArH), 8.02–8.05 (m, 2H, ArH), 7.53–7.56 (m, 2H, ArH), 7.27–7.30 (m, 2H, ArH), 4.61 (s, 2H, NH_2); HRMS calcd for $[M + H]^+$ $C_{14}H_{12}ClN_4O$: 287.0700; found: 287.0707.

*2.2.2.5. 2-Phenyl-pyrazolo [1,5-a]pyridine-5-carbohydrazide (**2e**).* White solid, yield 89%, mp 242–243 °C. ^{1}H NMR (300 MHz, d_6-DMSO): δ 10.00 (s, 1H, NH), 8.76–8.78 (d, J = 7.2 Hz, 1H, ArH), 8.18 (s, 1H, ArH), 8.00–8.03 (m, 2H, ArH), 7.38–7.51 (m, 3H, ArH), 7.25–7.29 (m, 2H, ArH), 4.59 (s, 2H, NH_2); HRMS calcd for $[M + H]^+$ $C_{14}H_{13}N_4O$: 253.1089; found: 253.1093.

*2.2.2.6. 2-(Naphthalen-2-yl)-pyrazolo [1,5-a]pyridine-5-carbohydrazide (**2f**).* White solid, yield 93%, mp 230–231 °C. ^{1}H NMR (300 MHz, d_6-DMSO): δ 10.03 (s, 1H, NH), 8.79–8.82 (d, J = 7.5 Hz, 1H, ArH), 8.59 (s, 1H, ArH), 8.16–8.23 (m, 2H, ArH), 7.94–8.04 (m, 3H, ArH), 7.52–7.59 (m, 2H, ArH), 7.42 (s, 1H, ArH), 7.28–7.31 (m, 1H, ArH), 4.64 (s, 2H, NH_2); HRMS calcd for $[M + H]^+$ $C_{18}H_{15}N_4O$: 303.1246; found: 303.1248.

Table 1
Crystal data and structure refinement for **3a**.

3a	
Empirical formula	$C_{23}H_{18}N_4O_3$
Formula weight	398.41
Temperature	298(2) K
Wavelength	0.71073 Å
Crystal system	Monoclinic
Space group	P 1 21/c 1
Unit cell dimensions	a = 19.962(8) Å, α = 90° b = 11.030(4) Å, β = 91.273(7)° c = 8.856(4) Å, γ = 90°
Volume	1949.44(140) Å^3
Z	4
Calculated density	1.3574 Mg/m^3
Absorption coefficient	0.093 mm^{-1}
F(000)	832
Crystal size	0.15 × 0.15 × 0.10 mm
θ range for data collection	2.04–27.38°
Limiting indices	$-13 \le h \le 25$ $-14 \le k \le 12$ $-10 \le l \le 10$
Reflections collected/unique	10,970/4311 [R(int) = 0.0214]
Completeness to θ = 27.56°	97.4%
Absorption correction	None
Max. and min. transmission	0.9908 and 0.9862
Refinement method	Full-matrix least-squares on F^2
Data/restraints/parameters	4311/0/320
Goodness-of-fit on F^2	0.998
Final R indices [$I > 2\sigma(I)$]	R_1 = 0.0413, wR_2 = 0.1147
R indices (all data)	R_1 = 0.0616, wR_2 = 0.1294
Largest diff. peak and hole	0.191 and −0.163 eÅ^{-3}

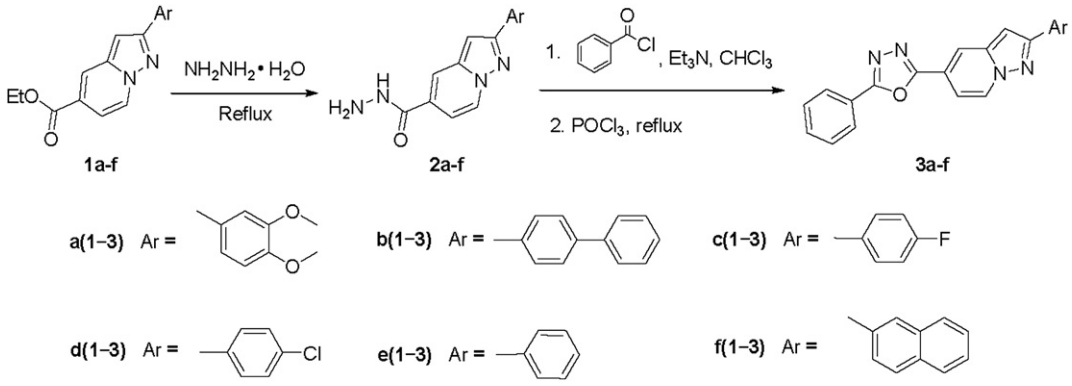

Fig. 2. Synthetic routes of **3a**–**f**.

*2.2.3. General procedure for the synthesis of **3a**–**f***

A solution of benzoyl chloride (2 mmol) in $CHCl_3$ (5 mL) was added dropwise into a $CHCl_3$ (10 mL) solution of compound **2** (2 mmol) and triethylamine (2 mmol) at room temperature. The resulting mixture was stirred for 5 h. The solvent was removed under vacuum and the crude product was washed with petroleum ether and water. The solid was dried and added to phosphorus oxychloride (caution: reacts violently with water; incompatible with many metals, alcohols, amines, phenol, DMSO, and strong bases) (10 mL). The mixture was refluxed for 12 h and cooled to room temperature. The solution was added dropwise into ice water (50 mL), and yellow solid was precipitated. The crude product was collected by filtration and washed with water. The solid was purified by chromatography (silica gel, hexane/ethyl acetate, 3/1, v/v).

*2.2.3.1. 2-(3,4-Dimethoxyphenyl)-5-(5-phenyl-1,3,4-oxadiazol-2-yl)-pyrazolo [1,5-a]pyridine (**3a**).* White solid, yield 73%, mp 397–398 °C. IR (KBr) ν/cm^{-1}: 3037 (ArH), 2995, 2836 (C–H in CH_3), 1253 (C–O–C), 730 (ArH); ^{1}H NMR (300 MHz, $CDCl_3$): δ 8.56–8.58 (d, J = 7.2 Hz, 1H, ArH), 8.27 (s, 1H, ArH), 8.15–8.18 (m, 2H, ArH), 7.47–7.58 (m, 6H, ArH), 6.95–6.98 (m, 2H, ArH), 4.02 (s, 3H), 3.95 (s, 3H); HRMS calcd for $[M + H]^+$ $C_{23}H_{19}N_4O_3$: 399.1457; found: 399.1449.

*2.2.3.2. 2-(4-Biphenyl)-5-(5-phenyl-1,3,4-oxadiazol-2-yl)-pyrazolo [1,5-a]pyridine (**3b**).* White solid, yield 77%, mp 413–414 °C. IR (KBr) ν/cm^{-1}: 3051 (ArH), 1447 (Ar), 760, 728 (ArH); ^{1}H NMR (300 MHz, $CDCl_3$): δ 8.60–8.62 (d, J = 7.2 Hz, 1H, ArH), 8.33 (s, 1H, ArH), 8.06–8.09 (m, 2H, ArH), 7.63–7.74 (m, 5H, ArH), 7.45–7.59 (m, 6H, ArH), 7.38–7.40 (m, 2H, ArH), 7.06 (s, 1H, ArH); HRMS calcd for $[M + H]^+$ $C_{27}H_{19}N_4O$: 415.1559; found: 415.1585.

*2.2.3.3. 2-(4-Fluorophenyl)-5-(5-phenyl-1,3,4-oxadiazol-2-yl)-pyrazolo [1,5-a]pyridine (**3c**).* White solid, yield 82%, mp 355–356 °C. IR (KBr) ν/cm^{-1}: 3050 (ArH), 1441 (Ar), 1227 (C–F), 791, 726 (ArH); ^{1}H NMR (300 MHz, $CDCl_3$): δ 8.57–8.59 (d, J = 7.2 Hz, 1H, ArH), 8.31 (s, 1H, ArH), 8.16–8.19 (m, 2H, ArH), 7.95–7.99 (m, 2H, ArH), 7.50–7.59 (m, 4H, ArH), 7.14–7.20 (m, 2H, ArH), 6.97 (s, 1H, ArH); HRMS calcd for $[M + H]^+$ $C_{21}H_{14}FN_4O$: 357.1152; found: 357.1137.

*2.2.3.4. 2-(4-Chlorophenyl)-5-(5-phenyl-1,3,4-oxadiazol-2-yl)-pyrazolo [1,5-a]pyridine (**3d**).* White solid, yield 80%, mp 371–372 °C. IR (KBr) ν/cm^{-1}: 3049 (ArH), 1436 (Ar), 1089 (C–Cl), 794 (ArH); ^{1}H NMR (300 MHz, $CDCl_3$): δ 8.59 (d, J = 7.2 Hz, 1H, ArH), 8.31 (s, 1H, ArH), 8.19 (m, 2H, ArH), 7.92–7.95 (m, 2H, ArH), 7.44–7.59 (m, 6H, ArH), 7.00 (s, 1H, ArH); HRMS calcd for $[M + H]^+$ $C_{21}H_{14}ClN_4O$: 373.0856; found: 373.0847.

*2.2.3.5. 2-Phenyl-5-(5-phenyl-1,3,4-oxadiazol-2-yl)-pyrazolo [1,5-a] pyridine (**3e**).* White solid, yield 88%, mp 337–338 °C. IR (KBr) ν/cm^{-1}: 3049 (ArH), 1563 (Ar), 763 (ArH), 682 (Ar); ^{1}H NMR (300 MHz, $CDCl_3$): δ 8.58–8.60 (d, J = 7.2 Hz, 1H, ArH), 8.30 (s, 1H, ArH), 8.15–8.19 (m, 2H, ArH), 7.98–8.01 (m, 2H, ArH), 7.53–7.60 (m, 3H, ArH), 7.38–7.52 (m, 4H, ArH), 7.02 (s, 1H, ArH); HRMS calcd for $[M + H]^+$ $C_{21}H_{15}N_4O$: 339.1246; found: 339.1238.

*2.2.3.6. 2-(Naphthalen-2-yl)-5-(5-phenyl-1,3,4-oxadiazol-2-yl)-pyrazolo [1,5-a]pyridine (**3f**).* White solid, yield 70%, mp 264–265 °C. IR (KBr) ν/cm^{-1}: 3048 (ArH), 1563 (Ar), 724 (ArH), 681 (Ar); ^{1}H NMR (300 MHz, $CDCl_3$): δ 8.63–8.65 (d, J = 7.5 Hz, 1H, ArH), 8.48 (s, 1H, ArH), 8.34 (s, 1H, ArH), 8.11–8.20 (m, 3H, ArH), 7.87–7.97 (m, 3H, ArH), 7.51–7.60 (m, 6H, ArH), 7.16 (s, 1H); HRMS calcd for $[M + H]^+$ $C_{25}H_{17}N_4O$: 389.1402; found: 389.1407.

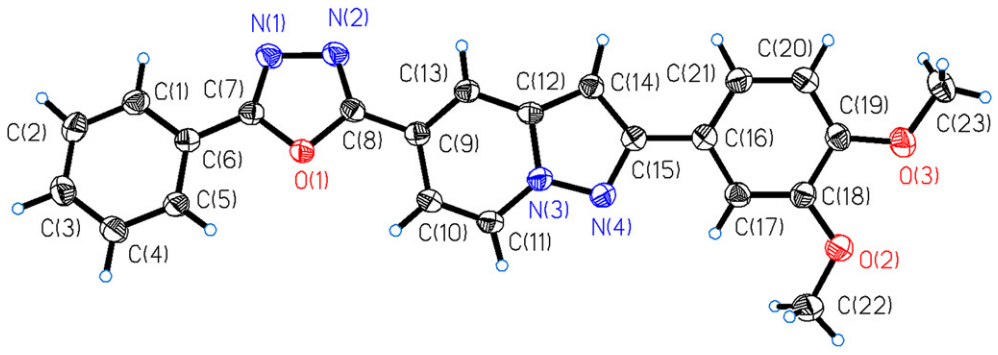

Fig. 3. The molecular structure of **3a** with displacement ellipsoids drawn at the 50% probability level.

Table 2
The selected bond lengths (Å) and bond angles (°) for compound **3a**.

O(1)–C(8)	1.3684(17)	C(9)–C(8)	1.462(2)
O(1)–C(7)	1.3727(17)	C(15)–C(16)	1.479(2)
N(3)–N(4)	1.3570(17)	O(2)–C(18)	1.3667(19)
N(3)–C(11)	1.373(2)	C(6)–C(7)	1.456(2)
N(2)–C(8)	1.2892(19)	N(4)–C(15)	1.3533(19)
N(2)–N(1)	1.4102(18)	O(2)–C(22)	1.422(2)
C(8)–O(1)–C(7)	102.90(11)	N(4)–N(3)–C(11)	124.78(13)
N(4)–N(3)–C(12)	112.54(12)	C(11)–N(3)–C(12)	122.66(13)
C(14)–C(12)–C(13)	137.01(14)	C(8)–N(2)–N(1)	106.48(12)
N(4)–C(15)–C(14)	111.89(14)	N(4)–C(15)–C(16)	119.61(13)
N(1)–C(7)–O(1)	111.88(13)	O(1)–C(7)–C(6)	118.90(12)
C(7)–N(1)–N(2)	106.54(12)	N(2)–C(8)–O(1)	112.19(13)
N(2)–C(8)–C(9)	128.31(13)	O(1)–C(8)–C(9)	119.47(12)

2.3. X-ray crystallography

Suitable single crystals of **3a** for X-ray structure analysis were obtained by slow evaporation of a solution of the solid in ethyl acetate. The diffraction data of crystals with approximate dimensions of 0.15 × 0.15 × 0.10 mm were collected with a Bruker-Nonius SMART APEX IICCD diffractometer using a graphite monochromated Mo Kα radiation (λ = 0.71073 Å) at 298(2) K. The structures were solved by direct methods with SHELXS-97 program and refinements on F^2 were performed with SHELXL-97 program by full-matrix least-squares techniques with anisotropic thermal parameters for the non-hydrogen atoms. All H atoms were initially located in a difference Fourier map. The methyl H atoms were then constrained to an ideal geometry, with C–H = 0.96 Å and $U_{iso}(H) = 1.5\ U_{eq}(C)$. All other H atoms were placed in geometrically idealized positions and constrained to ride on their parent atoms, with C–H = 0.93 Å and $U_{iso}(H) = 1.2\ U_{eq}(C)$. A summary of the crystallographic data and structure refinement details is given in Table 1.

3. Results and discussion

3.1. Synthesis and structure characterization

The synthetic route to the target heterocycles is shown in Fig. 2.

The starting materials **1a**–**f** can be easily prepared from 3-arylpyrazole-5-carbaldehyde and ethyl 4-bromobut-2-enoate in 76–87% yields by a tandem reaction we previously reported [25]. Compounds **1** reacted with hydrazine hydrate to afford compounds **2** in good yield. The compounds **2** then reacted with aryl chlorides in the presence of triethylamine, followed by dehydration in phosphorus oxychloride to give desired compounds **3**.

The assumed structures of target products were characterized by IR, ^{1}H NMR and HRMS spectra. For example compound **3a**, obtained as white solid, gave an [M + H]-ion peak at *m/z* 399.1449

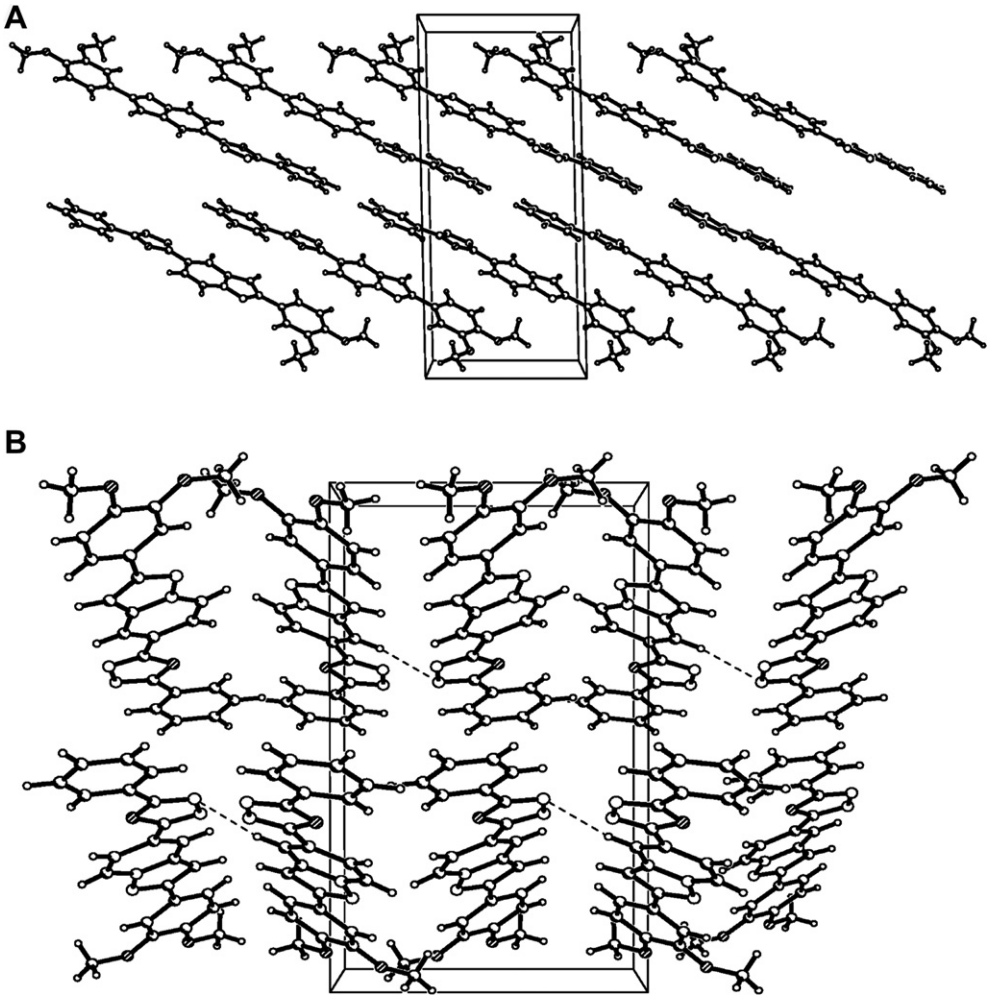

Fig. 4. Crystal packing diagram of **3a** along the *b*-axis (A) and *c*-axis (B).

Table 3
The absorption characteristics of compounds **1a**–**f** and **3a**–**f**.

Compounds	λ_{max} (nm)				ε_{max} (L mol^{-1} cm^{-1})			
	CH_2Cl_2		Cyclohexane		CH_2Cl_2		Cyclohexane	
1a	279	297	277	296	44,790	32,944	39,519	26,256
1b	290	–	289	–	63,995	–	58,125	–
1c	264	274	264	273	59,906	48,060	58,918	46,853
1d	270	279	269	280	57,664	49,299	55,952	46,060
1e	267	275	264	275	56,635	47,850	58,532	48,438
1f	267	298	266	296	71,775	33,131	70,008	31,212
3a	301	335	298	340	50,878	17,539	18,880	7116
3b	299	348	297	351	49,914	10,442	18,270	3232
3c	283	338	383	328	53,375	14,648	21,670	6145
3d	286	339	285	342	61,983	14,845	11,236	2261
3e	283	340	284	342	57,580	15,415	42,547	11,237
3f	303	349	290	351	47,811	13,312	5660	1401

in the HRMS, in accord with the molecular formula $C_{23}H_{19}N_4O_3$. The IR spectra of compound **3a** showed the characteristic absorption bands at 3037 cm^{-1} (ArH) and 1253 cm^{-1} (C–O–C). The ^{1}H NMR spectra ($CDCl_3$) of compound **3a** revealed two singlet peaks at δ 3.95 (3H, CH_3) and 4.02 (3H, CH_3) which were readily assigned to the hydrogen atoms of two methoxy moieties. The peaks between δ 6.98–8.58 for compound **3a** were also consistent with protons on aromatic rings. Moreover, the structure of compound **3a** was confirmed by X-ray diffraction analysis.

3.2. Crystal structure

The single crystal structure and atomic numbering chosen for compound **3a** are shown in Fig. 3. The structure of **3a** is in a monoclinic crystal system with a P1 21/c 1 space group. The pyrazolo[1,5-*a*]pyridine subunit is substantially planar with a dihedral angles of 2.70° between pyrazole and pyridine segments. The dihedral angles between the pyrazolo[1,5-*a*]pyridine ring and 1,3,4-oxadiazole or C16 phenyl ring are 11.25° and 7.50°, respectively. Furthermore, the dihedral angle between 1,3,4-oxadiazole ring and the C6 phenyl ring is 2.31°. All these dihedral angles are so small that the four rings in **3a** nearly construct a plane, providing a large conjugated system within the molecule. Selected bond lengths and bond angles are listed in Table 2. The results reveal that the carbon–carbon bond lengths on the molecular skeleton are basically intermediate between typical C–C single (1.54 Å) and C=C double (1.34 Å) bonds. The carbon–nitrogen bond lengths are also intermediate between typical C–N single (1.47 Å) and C=N double (1.27 Å) bonds. This indicates that the π-electrons in the molecule are delocalized.

The stacking structure of **3a** along the *b* and *c* axis of the unit cell is shown in Fig. 4. Compound **3a** packs in a herringbone arrangement with a dihedral angle between non-parallel molecules of 56.88°. The distance between two neighboring molecules, which have face to face parallel orientation to each other, is 6.4946 Å. The crystal packing structure also demonstrates the existence of intermolecular hydrogen bond between the C13–H13 on the pyrazolo[1,5-*a*]pyridine ring and N1 atom on the 1,3,4-oxadiazole ring with bond length of 2.4829 Å.

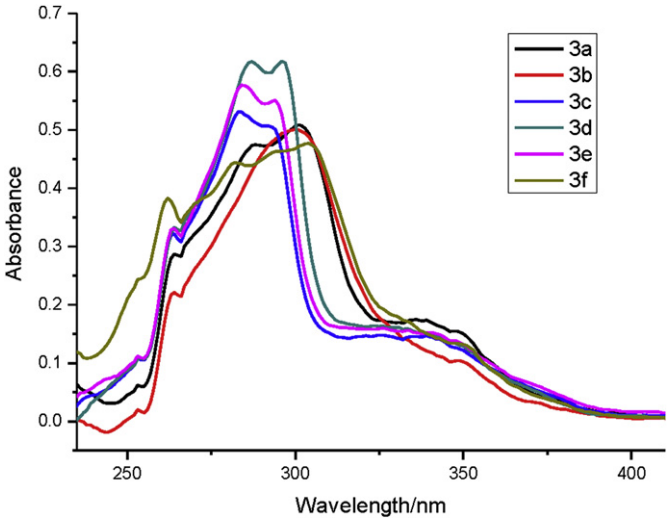

Fig. 6. UV–vis absorption spectrum of compounds **3a**–**f** in dichloromethane solution (1×10^{-5} mol L^{-1}).

3.3. Absorption spectral characteristics of the compounds *1a–1f and 3a–3f*

The UV–vis spectral data of the compounds **1a**–**f** and **3a**–**f** are summarized in Table 3. Fig. 5 shows the absorption spectrum of

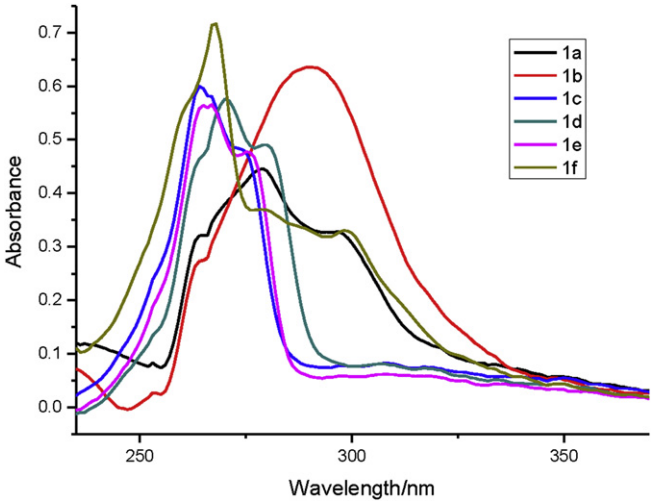

Fig. 5. UV–vis absorption spectrum of compounds **1a**–**f** in dilute (1×10^{-5} mol L^{-1}) dichloromethane solution.

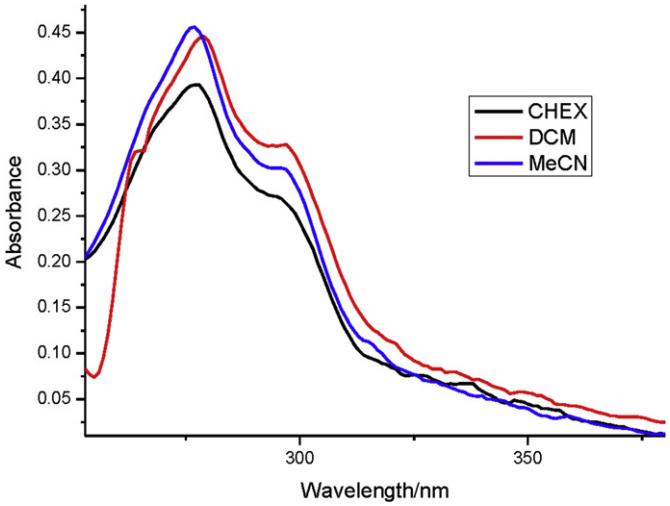

Fig. 7. UV–vis absorption spectrum of compound **1a** in different solvents.

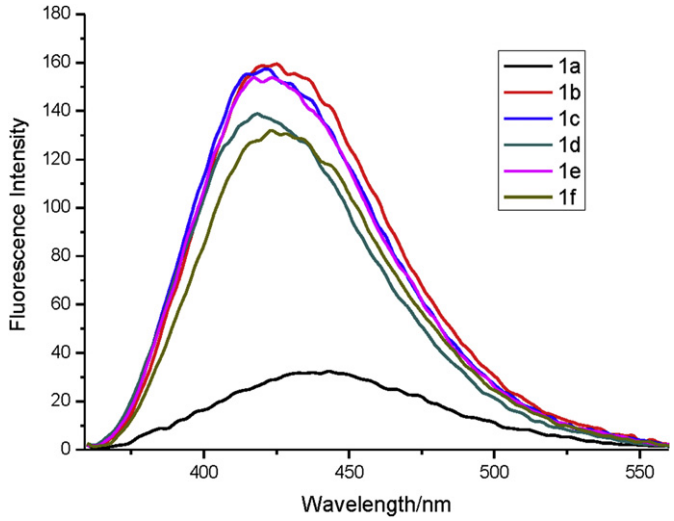

Fig. 8. Emission spectrum of compounds **1a**–**f** in dilute (1×10^{-5} mol L^{-1}) dichloromethane solution.

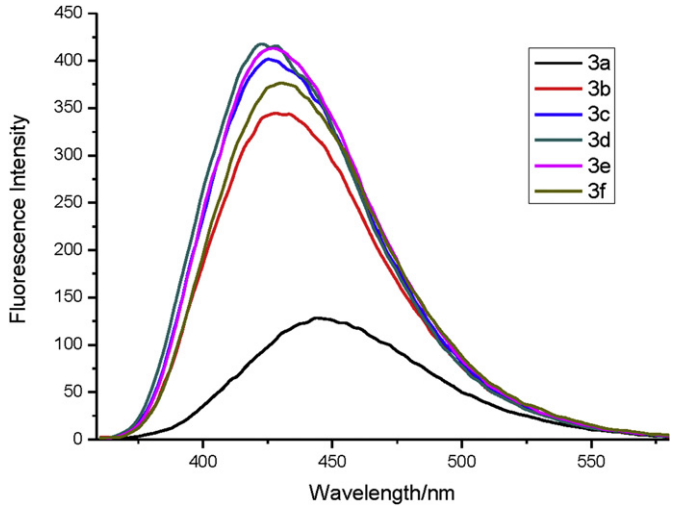

Fig. 9. Emission spectrum of compounds **3a**–**f** in dichloromethane solution (1×10^{-5} mol L^{-1}).

Table 4
Fluorescence spectral data for **1a**–**f** and **3a**–**f** in dichloromethane.

Compounds	λ_{max}^{ex} (nm)[a]	λ_{max}^{em} (nm)[a]	Stoke's shift (nm)[a]	Φ_{PL}[b]
1a	283	442	159	0.32
1b	291	426	135	0.60
1c	267	422	155	0.52
1d	272	421	149	0.57
1e	268	421	153	0.42
1f	264	423	159	0.48
3a	312	444	132	0.73
3b	298	428	130	0.83
3c	340	425	85	0.62
3d	332	422	90	0.46
3e	338	427	89	0.59
3f	339	430	91	0.58

[a] Solution in 1×10^{-5} mol L^{-1} CH_2Cl_2.
[b] Φ_{PL} is relative PL quantum efficiency of target compound solution in 1×10^{-6} mol L^{-1} CH_2Cl_2 which is determined by using 1×10^{-6} mol L^{-1} H_2SO_4 ($\Phi = 0.55$) as the standard reference.

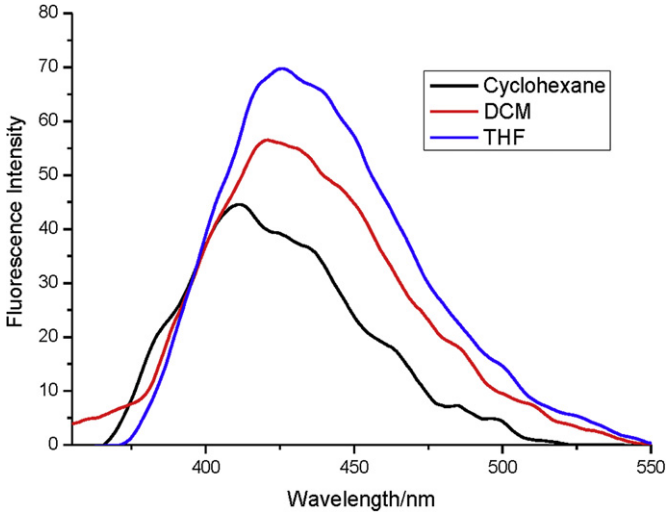

Fig. 10. The fluorescence spectra of compound **3d** in different solvents.

compounds **1a**–**f** in dichloromethane. The results show that **1a**–**f** display absorptions ranging from 235 to 340 nm, which are attributed to the π–π^* transition of conjugated backbone. Compounds **1c**, **1d**, **1e** and **1f** have similar absorption characteristics and present sharp absorption peaks at 264 nm, 270 nm, 267 nm and 267 nm, respectively, with shoulders at longer wavelengths of 274 nm for **1c**, 279 nm for **1d**, 275 nm for **1e** and 298 nm for **1f**. In the case of **1a**, it exhibits one sharp absorption peak at 279 nm, about 12 nm red-shifted compared with the corresponding peaks of **1e**, due to the strong electron-donating effect of two methoxy groups on 2-phenyl ring. Compound **1a** shows its shoulder absorption towards longer wavelength at 297 nm. It is worth noting that compound **1b** presents a broad absorption ranging from 250 nm to 340 nm, with absorption maxima red-shifted distinctly to 290 nm, resulting from the electron-donating effect of phenyl

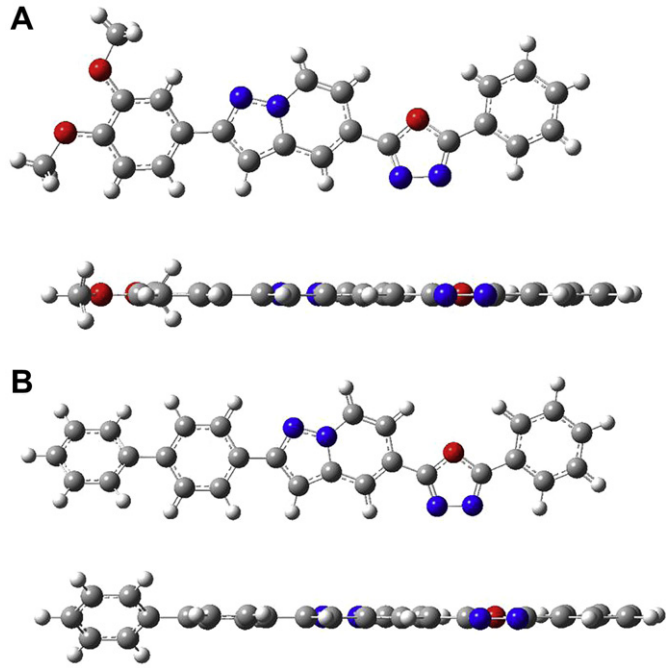

Fig. 11. The simplified molecular structures during the DFT calculation and the minimized structures of compounds **3a** (A) and **3b** (B).

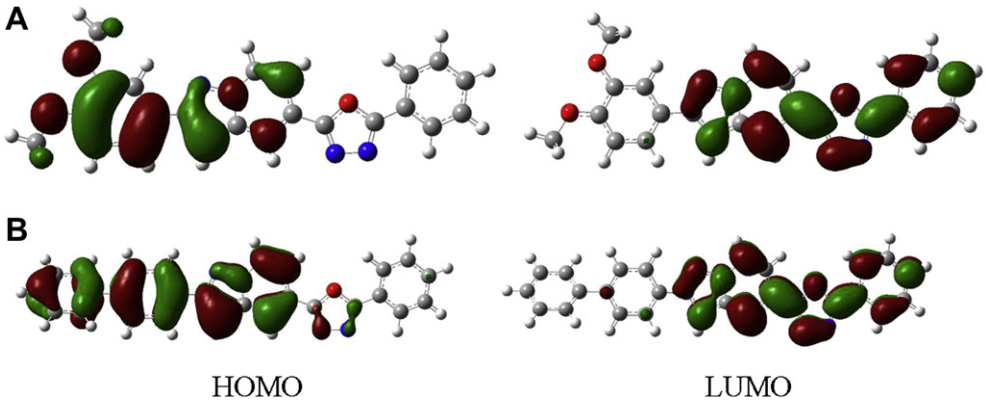

Fig. 12. Molecular orbital maps of compounds **3a** (A) and **3b** (B).

group on the 2-phenyl ring and the formation of a more delocalized and extended π-conjugated system.

For compounds **3a**–**f** (Fig. 6), they show absorption peaks at longer wavelengths compared with the corresponding ethyl 2-aryl-pyrazolo[1,5-*a*]pyridine-5-carboxylates (**1a**–**f**), which may be due to the extension of conjugation from 5-phenyl-1,3,4-oxadiazole segment. Compounds **3c**, **3d** and **3e** demonstrate similar absorption properties, with absorption peaks at 283 nm, 286 nm and 283 nm, respectively. The result reveals that halogen atoms (F or Cl) on 2-phenyl rings only slightly affect the absorption character of these 1,3,4-oxadiazole compounds. However, for compounds **3a**, **3b** and **3f** with strong electron-donating groups or a high degree of conjugation within their molecules, the absorption maxima are red-shifted to 301 nm, 299 nm and 303 nm, respectively. It should be noted that **3a**–**f** also present weak charge transfer absorption bands between 335 nm and 349 nm, attributed to charge transfer from pyrazolo[1,5-*a*]pyridine moiety to electron-accepting oxadiazole units.

Influence of solvent on the absorption behavior was investigated. The absorption spectra of **1a**, as an example, in three different solvents (cyclohexane, dichloromethane and acetonitrile) at a concentration of 1×10^{-5} mol L^{-1} are shown in Fig. 7. It is observed that the absorption spectra change slightly with the increase of solvent polarity although there is a tendency of a shorter λ_{max} in acetonitrile, indicating that there is no charge transfer in the ground state.

3.4. Fluorescence spectral characteristics

The emission spectra of compounds **1a**–**f** in CH_2Cl_2 are shown in Fig. 8. They present efficient blue emissions in dilute solution, with maximum emission spectra ranging from 421 to 442 nm. It can be found that their intensity of fluorescence differed from each other. The fluorescence intensity of compound **1a** is extremely weak compared with other compounds, which may be due to the interaction of molecules leading to the quenching of fluorescence at the measured concentration of 1×10^{-5} mol L^{-1}. For compound **1a**, the Donor–Acceptor structure character resulting from the electron-donating methoxy groups and electron-withdrawing ester group is in favor of dipole–dipole interactions between molecules.

The maximum emissions of compounds **3a**–**f** are similar to **1a**–**f**, as demonstrated in Fig. 9. But the fluorescence intensity is stronger than the corresponding intensity of **1a**–**f**. The Stoke's shift and fluorescence quantum yields of these compounds are summarized in Table 4. Compounds **1a**–**f** and **3a**–**f** show moderate fluorescence quantum yields ranging from 0.32 to 0.83. The result reveals that **3a**–**f** exhibit higher Φ_{PL} than **1a**–**f**, which may be caused by the incorporation of oxadiazole moiety into the molecules. The Stoke's shifts of compounds **1a**–**f** and **3a**–**f** range from 85 to 159 nm, indicating the existence of molecular conformation deviation between the ground state and the exited state.

The solvent effects on the fluorescence characteristics of these compounds were investigated in cyclohexane, CH_2Cl_2 and THF at the concentration of 1×10^{-5} mol L^{-1}. For compound **3d** in Fig. 10, the emission wavelengths are red shifted with the increase of solvent polarity from 411 nm in cyclohexane to 420 nm in CH_2Cl_2 and 426 nm in THF. Due to the interaction between fluorescent molecules and solvent, the fluorescence is also enhanced with the increase of solvent polarity.

3.5. Theoretical calculation

Density functional theory (DFT) calculations (B3LYP; 6-31G*) set in the Gaussian 03 program package [27] were carried out to obtain information about the HOMO and LUMO distributions of these compounds. As examples, the minimized structures of **3a** and **3b** are shown in Fig. 11 and their calculated molecular orbital (HOMO and LUMO) energies are shown in Fig. 12. The minimized structure of compound **3a** reveals that all aromatic rings are strictly coplanar, which is different from the molecular conformation in the crystal structure, with an energy difference of 0.79 kJ mol^{-1}. The conformation deviation may results from hydrogen bond existing in the crystal structure, as demonstrated in Fig. 4. For compound **3b**, the theoretical model indicates a dihedral angle of 37.3° within its biphenyl unit while other aromatic rings present in the same plane.

The molecular energy levels of the frontier molecular orbital shown in Fig. 12 illustrates that HOMOs are π orbitals concentrating on the 2-aryl-pyrazolo[1,5-*a*]pyridine moieties and LUMOs are of π* character distributing in the electron-accepting 5-(5-phenyl-1,3,4-oxadiazol-2-yl)-pyrazolo[1,5-*a*]pyridine segments. It should be noted that the HOMO distributes in 3,4-dimethoxyphenyl ring at a larger degree for compound **3a** than that in biphenyl group for compound **3b**, due to the strong electron-donating property of methoxyl group.

4. Conclusions

A series of novel 2,5-diaryl-1,3,4-oxadiazole derivatives containing pyrazolo[1,5-*a*]pyridine moiety have been synthesized and their structures were characterized by IR, ^1H NMR and HRMS spectra. Representatively, the spatial structure of compound **3a** was determined by X-ray diffraction analysis. The absorption maxima of compounds **1a**–**f** vary from 264 nm to 290 nm depending on the groups bonded to benzene rings. Compounds **3a**–**f** show

red-shifted absorption peaks ranging from 283 to 303 nm compared to the corresponding absorption of **1a**–**f**, due to their extended conjugation. The maximum emission spectra of the target compounds range from 421 to 444 nm and compounds **3** have higher fluorescence quantum yields (Φ_{PL} = 0.46–0.83) than corresponding those of compounds **1** (Φ_{PL} = 0.32–0.60). These small molecules have potential bioactivities and fluorescent properties, and their use as fluorescent pigments and electroluminescent materials are currently under investigation.

Acknowledgements

The authors thank the Shandong Natural Science Foundation (No. Y2008B40) and Shandong Excellent Young and Mid-aged Scientist Promotive Foundation (No. 2008BS04024) for financial support of this work.

Appendix. Supplementary materials

CCDC 787181 contains the supplementary crystallographic data for this paper. These data can be obtained free of charge via http://www.ccdc.cam.ac.uk/data_request/cif, by emailing data_request@ccdc.cam.ac.uk, or by contacting The Cambridge Crystallographic Data Centre, 12, Union Road, Cambridge CB21EZ, UK; fax: +44 1223 336033.

References

[1] Schulz B, Bruma M, Brehmer L. Adv Mater 1997;9:601–13.
[2] Jin SH, Kim MY, Kim JY, Lee K, Gal YS. J Am Chem Soc 2004;126:2474–80.
[3] Leung MK, Yang CC, Lee JH, Tsai HH, Lin CF, Huang CY, et al. Org Lett 2007;9:235–8.
[4] Lee DW, Kwon KY, Jin JI, Park Y, Kin YR, Hwang IW. Chem Mater 2001;13:565–74.
[5] Hughes G, Bryce MR. J Mater Chem 2005;15:94–107.
[6] Kulkarni AP, Tonzola CJ, Babel A, Jenekhe SA. Chem Mater 2004;16:4556–73.
[7] Kim OK, Lee KS, Woo HY, Kim KS, He GS, Swiatkiewicz J, et al. Chem Mater 2000;12:284–6.
[8] Huang PH, Shen JY, Pu SC, Wen YS, Lin JT, Chou PT, et al. J Mater Chem 2006;16:850–7.
[9] Qian Y, Meng K, Lu CG, Lin BP, Huang W, Cui YP. Dyes Pigm 2009;80:174–80.
[10] Goudreault T, He Z, Guo Y, Ho CL, Zhan H, Wang Q, et al. Macromolecules 2010;43:7936–49.
[11] Landis CA, Dhar BM, Lee T, Sarjeant A, Katz HE. J Phys Chem C 2008;112:7939–45.
[12] Lee T, Landis CA, Dhar BM, Jung BJ, Sun J, Sarjeant A, et al. J Am Chem Soc 2009;131:1692–705.
[13] Li AF, Ruan YB, Jiang QQ, He WB, Jiang YB. Chem Eur J 2010;16:5794–802.
[14] Fang YK, Liu CL, Li C, Lin CJ, Mezzenga R, Chen WC. Adv Funct Mater 2010;20:3012–24.
[15] Bettinetti L, Schlotter K, Hubner H, Gmeiner P. J Med Chem 2002;45:4594–7.
[16] Prante O, Tietze R, Hocke C, Lober S, Hubner H, Kuwert T, et al. J Med Chem 2008;51:1800–10.
[17] Lober S, Aboul-Fadl T, Hubner H, Gmeiner P. Bioorg Med Chem Lett 2002;12:633–6.
[18] Ehrlich K, Gotz A, Bollinger S, Tschammer N, Bettinetti L, Harterich S, et al. J Med Chem 2009;52:4923–35.
[19] Akahane A, Katayama H, Mitsunaga T, Kato T, Kinoshita T, Kita Y, et al. J Med Chem 1999;42:779–83.
[20] Cheung M, Harris PA, Badiang JG, Peckham GE, Chamberlain SD, Alberti MJ, et al. Bioorg Med Chem Lett 2008;18:5428–30.
[21] Qiao L, Choi S, Case A, Gainer TG, Seyb K, Glicksman MA, et al. Bioorg Med Chem Lett 2009;19:6122–6.
[22] Gudmundsson KS, Johns BA, Allen SH. Bioorg Med Chem Lett 2008;18:1157–61.
[23] Allen SH, Johns BA, Gudmundsson KS, Freeman GA, Boyd Jr FL, Sexton CH, et al. Bioorg Med Chem 2006;14:944–54.
[24] Marder SR, Stucky GD, Sohn JE. ACS symposium series, vol. 455. Washington, DC: ACS; 1991.
[25] Ge YQ, Jia J, Li Y, Yin L, Wang JW. Heterocycles 2009;78:197–206.
[26] Ge YQ, Jia J, Yang H, Tang XT, Wang JW. Dyes Pigm 2011;88:344–9.
[27] Frisch MJ, Trucks GW, Schlegel HB, Scuseria GE, Robb MA, Cheeseman JR, et al. Gaussian 03, revision A. 1. Pittsburgh, PA: Gaussian, Inc.; 2004.